Pinning of a two-dimensional membrane on top of a patterned substrate: The case of graphene

S. Viola Kusminskiy,[1,*] D. K Campbell,[1] A. H. Castro Neto,[1] and F. Guinea[2]
[1]*Department of Physics, Boston University, 590 Commonwealth Avenue, Boston, Massachusetts 02215, USA*
[2]*Instituto de Ciencia de Materiales de Madrid, CSIC, Sor Juana Ines de la Cruz 3, E-28049 Madrid, Spain*
(Received 22 July 2010; revised manuscript received 18 January 2011; published 8 April 2011)

We study the pinning of a two-dimensional membrane to a patterned substrate within elastic theory both in the bending rigidity and in the strain-dominated regimes. We find that both the in-plane strains and the bending rigidity can lead to depinning. We show from energetic arguments that the system experiences a first-order phase transition between the attached configuration to a partially detached one when the relevant parameters of the substrate are varied, and we construct a qualitative phase diagram. Our results are confirmed through analytical solutions for some simple geometries of the substrate's profile. We apply our model to the case of graphene on top of a SiO_2 substrate and show that typical orders of magnitude for corrugations imply graphene will be partially detached from the substrate.

DOI: 10.1103/PhysRevB.83.165405 PACS number(s): 68.55.−a, 68.65.Pq, 68.35.Rh

I. INTRODUCTION

Until recently, the study of two-dimensional (2D) membranes was developed mainly for its theoretical interest and its applications to biological systems that could be well approximated by the 2D membrane model, as well as soft matter systems.[1] Nowadays, however, with the experimental discovery of graphene[2–5] (a two-dimensional graphite sheet), we have the opportunity of studying a truly 2D membrane. It has been proven that the membrane aspect of graphene, and in particular the presence or not of a substrate, plays an essential role in characterizing its behavior.[6–8] Graphene presents intrinsic ripples,[9] inherent to its 2D nature, that can interact with the propagating electrons and affect transport properties.[10] In most experimental settings to date, though, graphene is deposited on top of a substrate, either purposely patterned or presenting random disorder. A relevant question then is to determine how the spatial structure of the substrate affects that of graphene. This kind of study also opens the possibility of controlling the properties of graphene by patterning appropriately the substrate. Experiments have shown that the morphology of a graphene membrane on top of a substrate is largely determined by the substrate's profile,[11–14] as opposed to suspended graphene. The attachment of graphene to a corrugated surface leads to the bending and stretching of the graphene layer, so that the depinning of the layer may become energetically favorable. For device construction, as well as for the interpretation of experimental data, it is important to know if the graphene sheet is completely pinned to the substrate or if there are regions for which depinning occurs and graphene is suspended.

Given its experimental relevance, in this work we address the problem of determining which is the stable configuration of a membrane on top of a substrate that presents either depressions or protrusions. Although we will treat the problem in the context of graphene physics, our results are general. We analyze this problem from a general field theory framework, in which we show the possibility of a phase transition between a pinned configuration to a partially depinned one, where relevant parameters of the patterned substrate act as control parameters. We turn then to analyzing some simple substrate geometries that allow for analytical solutions. We will show that these examples quantitatively confirm our phenomenological, qualitative model. To the best of our knowledge, our work is the first in the graphene literature that takes into account the effect of in-plane strains for detachment of the membrane. We show that there is a length scale for the substrate's pattern beyond which the in-plane strains are dominant and can lead to depinning. This length scale marks the crossover from a regime in which the bending rigidity of the membrane is dominant energetically.

In what follows, we will analyze the depinning of a membrane from the substrate for the two different limiting regimes mentioned above. [Previous works have studied this problem for graphene restricted to the bending rigidity dominated (BD) regime and for some particular patterns of the substrate.[34–36] A comprehensive treatment of the problem of adhesion of a membrane to a substrate, in the BD regime, can be found in Refs. 16 and 37.] First, in Sec. II we introduce the model for the free energy of a membrane on top of a substrate, and by means of scaling arguments we establish the possibility of a phase transition for the system between two possible stable equilibrium configurations: the membrane being completely attached to the substrate or being partially detached. From this we are able to construct a qualitative phase diagram for the system. In the following sections, we proceed to a quantitative analysis for a given geometry of the substrate profile. We consider a substrate with a Gaussian depression or protuberance, and we obtain analytical solutions for the two limiting regimes: the bending rigidity dominated regime in Sec. III and the strain dominated regime in Sec. IV. In both cases, we show that the system presents a first-order phase transition from pinned to depinned as the ratio of width to height of the substrate's profile is varied. A discussion and possible experimental consequences are presented in Sec. V.

II. MODEL AND QUALITATIVE PHASE DIAGRAM

We consider a tethered membrane that lies on top of a substrate. We use the de Monge parametrization,[15] by which the membrane is parametrized by $(\mathbf{x}, h(\mathbf{x}))$, where h is the height with respect to some reference plane and $\mathbf{x} = (x, y)$ are the in-plane coordinates. In the same way, the profile of the

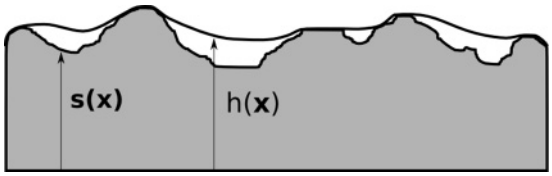

FIG. 1. Pictorial representation of a membrane on top of a random substrate, partially conforming to the substrate. The height of the membrane is represented by a field $h(\mathbf{x})$ while the top surface of the substrate is represented by a field $s(\mathbf{x})$, as discussed in the main text.

substrate is represented by $(\mathbf{x},s(\mathbf{x}))$, as shown schematically in Fig. 1.

We assume as a first approximation that the membrane couples to the substrate through its out-of-plane modes (also denominated flexural modes) via a contact force characterized by a surface tension γ_S. Previous works that study the attachment of a membrane to a substrate have used the so called Deryagin approximation, which approximates the interaction potential between the membrane and the substrate as a harmonic potential.[16] However, this approximation results in a strongly confining potential. In our case, we are interested in studying the stability of the pinned configuration and the possibility of detachment, and therefore a contact force approximation is more appropriate. Moreover, the interaction between graphene and a substrate has been studied in Ref. 17, and it has been shown that the attractive interaction force decays as the inverse distance to a power that depends on the type of interaction (a power of 2 in the case of undoped SiO_2). In that work, it was also shown that the coupling strength decays roughly four orders of magnitude when the graphene sheet is not pinned to the substrate. These considerations justify the use of a contact force that is finite when graphene is conforming to the substrate and zero otherwise. This is, of course, an idealization of our model since we are disregarding the equilibrium distance between the substrate and the membrane, which for graphene on a SiO_2 substrate is of the order of 5 Å.[11] The free energy for the membrane on top of the substrate within this approximation is given by

$$\mathcal{F}[\mathbf{u},h,s] = \frac{1}{2}\int d^2x[\kappa(\nabla^2 h(\mathbf{x}))^2 + 2\mu\tilde{u}_{ij}(\mathbf{x})^2 + \lambda\tilde{u}_{ii}(\mathbf{x})^2] - \frac{1}{2}\gamma_S\int_{\mathcal{S}} d^2x, \quad (1)$$

where μ and λ are the Lamé coefficients, κ is the bending rigidity of the membrane, and $\mathcal{S}$ is the surface of contact between the membrane and the substrate. Throughout this paper, we will use the accepted values of the elastic and bending parameters for graphene at room temperature. The bending rigidity is given by $\kappa \approx 1$ eV (Ref. 18) and the Lamé coefficients are given by $\mu \approx 10$ eV Å^{-2} and $\lambda \approx 2$ eV Å^{-2}.[19] We take the value of the coupling-constant strength as $\gamma_S = 2$ meVÅ^{-2}, corresponding to the maximum estimated pinning strength for graphene on a SiO_2 substrate.[17] (The value of $\gamma_S \approx 2$ meV Å^{-2} is actually an upper limit for γ_S, attained when there is a layer of water between graphene and the substrate.[17] Also, repulsive forces not considered in Ref. 17 would effectively reduce the value of γ_S.) The functional dependence of $\mathcal{F}[\mathbf{u},h,s]$ on the substrate's profile field $s(\mathbf{x})$ is given implicitly through the contact term, being $h(\mathbf{x}) \equiv s(\mathbf{x})$ when the membrane is attached to the substrate. $(\nabla^2 h(\mathbf{x}))^2$ is the local mean curvature of the membrane, and the *local* intrinsic curvature is encoded in the strain tensor: $\tilde{u}_{ij} = \frac{1}{2}(\partial_i \mathbf{u}_j + \partial_j \mathbf{u}_i + \partial_i h \partial_j h)$, with $\mathbf{u}(\mathbf{x})$ the in-plane phonon modes and the i, $j = 1,2$ index the two components of the field. [Note that although the *total* Gaussian curvature of a nearly flat 2D membrane is zero, the quartic interaction term generated by integrating out the in-plane phonon modes can be seen as a long-range interaction between the *local* Gaussian curvatures at different points in the membrane (see Ref. 15). This long-range interaction is responsible for the stability of a low-temperature flat phase in 2D membranes (see Refs. 1 and 20).] Since the action is quadratic in these modes, they can be integrated out[20] to obtain an effective free energy $e^{-\mathcal{F}_{\rm eff}[h,s]} = \int \mathcal{D}\mathbf{u} e^{-\mathcal{F}[\mathbf{u},h,s]}$ with

$$\mathcal{F}_{\rm eff}[h,s] = -\frac{\gamma_S}{2}\int_{\mathcal{S}} d^2x + \frac{\kappa}{2}\int d^2x(\nabla^2 h(\mathbf{x}))^2 + \frac{\mathrm{E}_{\rm 2D}}{8}\int d^2x\left[P^T_{ij}\partial_i h(\mathbf{x})\partial_j h(\mathbf{x})\right]^2, \quad (2)$$

where $P^T_{ij} = \delta_{ij} - \frac{\partial_i\partial_j}{\nabla^2}$ is the transverse projector and where we have used the expression for the Young modulus in 2D, $\mathrm{E}_{\rm 2D} = \frac{4\mu(\mu+\lambda)}{2\mu+\lambda}$. We are interested in analyzing the possible detachment of the graphene sheet from the substrate, and, in particular, finding the configuration that is energetically favorable. The general procedure would be to minimize the free energy Eq. (2) given a profile of the substrate to find the stable solution. However, the nonlinearity of Eq. (2) makes this program impossible to follow analytically, even for the most simple geometries. We are then obliged to make use of approximations if we are to make any analytical progress. It is usually assumed that the in-plane stresses are small and therefore their contribution, encapsulated in the quartic order term of the effective energy $\mathcal{F}_{\rm eff}[h,s]$, can be neglected. However, this is true only if the height fluctuations are not too big, as we proceed to show. If we consider a substrate of average height fluctuations S over a length scale L, from Eq. (1) we see that the bending energy of a membrane attached to this substrate scales as

$$E_K \sim \kappa\int d^2x(\nabla^2 h(\mathbf{x}))^2 \sim \frac{\kappa}{L^2}S^2, \quad (3)$$

where we have used that $\nabla \sim L^{-1}$ and the area $\int d^2x \sim L^2$. On the other hand, by similar arguments (note that $\tilde{u}_{ij} \sim S^2/L^2$), the elastic energy due to in-plane strains is given roughly by

$$E_{\rm el} \sim \frac{\mathrm{E}_{\rm 2D}}{L^2}S^4. \quad (4)$$

Therefore, the elastic energy due to in-plane strains is the main contribution to the total energy of the membrane if $\mathrm{E}_{\rm 2D}\bar{s}^2 \gg \kappa$. This analysis is valid except for quasi-one-dimensional (1D) geometries, where the height profile of the substrate is constant along one direction. For this case it is easy to show that the in-plane strains are completely screened by the height fluctuations and hence the in-plane stresses are zero, and the

only contribution to the elastic energy is due to the bending rigidity.

With the previous analysis, we have then arrived to a length scale

$$\ell = \sqrt{\frac{\kappa}{\mathrm{E_{2D}}}} \tag{5}$$

that determines a crossover from a *bending rigidity* dominated regime (BD regime) for $S < \ell$ to a *strain* dominated regime (SD regime) for $S > \ell$. With the values for the elastic parameters of graphene given above, $\ell \approx 1$ Å (compare with the temperature-dependent crossover length scale obtained by the renormalization of the bending rigidity due to the in-plane modes; see Refs. 1 and 38). Note that this scale is of the order of magnitude of the lattice spacing, and in principle this would imply that the BD regime for graphene is greatly suppressed.[21] However, recent atomistic simulations have shown that thermal height fluctuations of this magnitude are possible.[22] Moreover, the study presented in Ref. 22 shows that the continuum model can still be applied in this limit. This scale can thus be realized in graphene,[11,12] and therefore the crossover is of experimental relevance.

We can now study the two limiting regimes separately. For the BD regime, the free energy for the membrane can be approximated by

$$\mathcal{F}_{\mathrm{eff}}[h,s] \approx -\frac{\gamma_S}{2}\int_{\mathcal{S}} d^2x + \frac{\kappa}{2}\int d^2x \left(\nabla^2 h(\mathbf{x})\right)^2. \tag{6}$$

To solve for the equilibrium configuration, we look for the saddle-point solutions of Eq. (6) with a partially detached membrane and study their stability. Minimizing with respect to the height $h(\mathbf{x})$ yields the biharmonic equation within the detached region:

$$(\nabla^2)^2 h(\mathbf{x}) = 0, \tag{7}$$

to be solved together with the appropriate boundary conditions, while $h(\mathbf{x}) \equiv s(\mathbf{x})$ in the pinned region. The boundary conditions have to be imposed at the boundary of the surface $\mathcal{S}$, which is the curve at which the membrane starts to detach from the substrate. If we parametrize this closed curve by $\mathbf{x}^* \equiv \partial\mathcal{S}$, the boundary conditions are given by

$$h(\mathbf{x}^*) = s(\mathbf{x}^*), \tag{8}$$

$$\nabla h(\mathbf{x}^*) = \nabla s(\mathbf{x}^*). \tag{9}$$

The curve $\mathbf{x}^*$ itself is unknown and can be determined by an extra boundary condition, which implies a discontinuity in the second derivatives due to the surface tension force at the curve of detachment $\mathbf{x}^*$:[23]

$$\gamma_S = \kappa[\nabla^2 h(\mathbf{x}^*) - \nabla^2 s(\mathbf{x}^*)]^2. \tag{10}$$

Alternatively, it is equivalent to find the extrema of the free energy Eq. (6) as a function of $\mathbf{x}^*$. For a given arbitrary profile of the substrate $s(\mathbf{x})$, it is to be expected that the free energy will have many extrema, corresponding to unstable and metastable configurations. The curve $\mathbf{x}_0^*$ corresponding to a global minimum will give the stable equilibrium configuration; if this is the null curve, then the stable configuration is the totally pinned membrane. We see then that the curve $\mathbf{x}^*$ emerges as a natural order parameter of the problem between two possible states of the system: a null curve $\mathbf{x}_0^* \equiv 0$ corresponding to a membrane that is completely attached to the substrate, and a finite value of the function $\mathbf{x}_0^*$ which gives a partially detached membrane. A scalar order parameter can be obtained, for example, by taking the total length of the curve $|\mathbf{x}^*|$ (note that in this general context, the curve $\mathbf{x}^*$ can be disconnected). Our analytical results for the particular geometries studied, to be developed in the following sections, show that the pinned configuration is always at least a metastable minimum, and hence the pinned-to-depinned transition is always of first order. We can argue that this has to be true in general for smoothly corrugated substrates as follows. If we consider a small deviation of the system from the totally attached configuration $|\mathbf{x}_0^*| = 0$, described by a small detachment curve $|\delta\mathbf{x}^*|$, the energy cost due to depinning is proportional to the minimal area enclosed by the curve, $\sim|\delta\mathbf{x}^*|^2$. On the other hand, the smoothness of the substrate implies that, for small enough $|\delta\mathbf{x}^*|$, the area delimited by this curve is locally flat and hence the gain in energy due to the relaxation of bending and stretching of the membrane is negligible. Hence the pinned configuration is always a local minimum of the energy, and the phase transition to a partially detached configuration is of first order due to the development of new metastable states with the variation of the control parameters. It is safe to assume that, for fixed external conditions, these control parameters will be related to the characteristic width and height of the substrate's corrugations. To simplify the analysis, we can consider the problem of a single depression or protuberance in the substrate. Intuitively it is to be expected that the stability of the pinned configuration, given a coupling strength γ_S and bending rigidity κ, will depend on the aspect ratio of the substrate's profile. A simple energetic argument gives an estimate for this threshold. The interaction energy between the graphene layer and the substrate in a region of area L^2 is

$$E_{\mathrm{pin}} \sim \gamma_S L^2, \tag{11}$$

while, as we saw previously, the bending energy cost of height corrugations of scale S is given by Eq. (3). The change between the regime where the pinning energy is dominant and the layer is attached to the substrate, and the regime where the cost in bending energy leads to the detachment of the layer, is governed by the ratio

$$\frac{E_{\mathrm{pin}}}{E_K} \sim \frac{\gamma_S}{\kappa}\frac{L^4}{S^2}. \tag{12}$$

The membrane will prefer to attach to the substrate in the limit $\frac{E_{\mathrm{pin}}}{E_K} > 1$, which translates into a condition for the substrate profile:

$$\frac{S}{L^2} < \sqrt{\frac{\gamma_S}{\kappa}}, \tag{13}$$

indicating that pinning is favored for shallower depressions.

Within the bending rigidity approximation, detachment can occur due to the high bending energy cost that competes with the energy gain due to pinning. In the opposite regime, $S > \ell$, the in-plane stresses are dominant and we should consider the

possible detachment due to these modes. For this case, the free energy (1) can be approximated by

$$\mathcal{F} \approx -\frac{\gamma_S}{2}\int_S d^2x + \frac{1}{2}\int d^2x[2\mu\tilde{u}_{ij}(\mathbf{x})^2 + \lambda\tilde{u}_{ii}(\mathbf{x})^2]. \quad (14)$$

In this limit, the approximate free energy given by Eq. (14) still contains the nonlinear coupling between the in-plane and out-of-plane modes, and hence further approximations are necessary for obtaining analytical results (note that we have to retain the nonlinear term in the strain tensor since we are in the limit of large out-of-plane fluctuations). We will introduce these approximations in Sec. IV when we solve the system for a particular geometry of the substrate. For now, however, we can perform a scaling analysis similar to the one we did for the bending energy to determine a threshold energy for the pinned-to-depinned transition due to in-plane strains, depending on the aspect ratio of the perturbation in the substrate. In this case, the transition is controlled by the ratio of pinning energy to elastic energy:

$$\frac{E_{\text{pin}}}{E_{\text{el}}} \sim \frac{\gamma_S}{\mathrm{E}_{2\mathrm{D}}}\frac{L^4}{S^4}, \quad (15)$$

where we have used Eqs. (4) and (11). As in the previous case, we can argue that the membrane will favor the pinned configuration when $\frac{E_{\text{pin}}}{E_{\text{el}}} > 1$, which gives us the condition

$$\frac{S}{L} < \left(\frac{\gamma_S}{\mathrm{E}_{2\mathrm{D}}}\right)^{1/4}, \quad (16)$$

again consistent with the intuitive picture that shallower depressions should favor pinning. The possible equilibrium solutions for the curve of detachment $|\mathbf{x}^*|$ are given in this case by the extrema of the free energy Eq. (14). As in the BD regime, a globally stable solution with $|\mathbf{x}^*| = 0$ corresponds to the completely pinned configuration.

Equations (13) and (16) define two lines of critical values given by $S_c \equiv S(L_c)$, which mark the transition from pinned to depinned in the parameter space of height and width of the substrate's profile. Note that while in the BD regime the dependence of S_c on the critical width L_c is quadratic [see Eq. (13)], in the SD regime this dependence is linear. In the intermediate region, therefore, a crossover is to be expected between the two critical lines. These considerations allow us to construct a qualitative phase diagram. For this, it is useful to consider the dimensionless quantities $S \to S/\ell$, $L \to L/\ell$ that give the height and width of the substrate's profile in units of the length scale ℓ of the BD to SD regime crossover defined in Eq. (5). We can then write the critical lines as

$$\begin{aligned} S_c &= \ell\sqrt{\frac{\gamma_S}{\kappa}}L_c^2, \quad S_c \ll 1, \\ S_c &= \left(\frac{\gamma_S}{\mathrm{E}_{2\mathrm{D}}}\right)^{1/4} L_c, \quad S_c \gg 1. \end{aligned} \quad (17)$$

The qualitative phase diagram is shown in Fig. 2.

Near the critical line, the free energy Eq. (1) can be written as a Landau functional of the order parameter $|\mathbf{x}|$:

$$\mathcal{F}[|\mathbf{x}|] = A_2|\mathbf{x}^*|^2 + A_3|\mathbf{x}^*|^3 + \cdots + A_n|\mathbf{x}^*|^n, \quad (18)$$

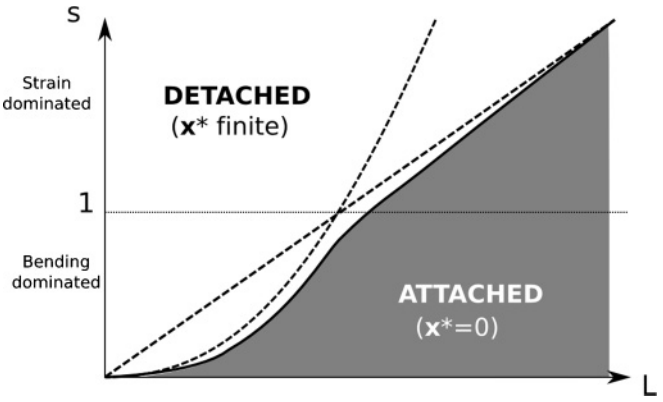

FIG. 2. Qualitative phase diagram for a membrane on top of a patterned substrate of characteristic width L and height S, in units of the length scale ℓ. The dashed lines correspond to the critical lines given by Eq. (17), the solid line is an estimated interpolation. Note that this phase diagram is not valid for 1D geometries, as discussed in the text.

where A_2 is a positive constant (in accordance with $|\mathbf{x}_0^*| = 0$ being always a local minimum) and the coefficients A_i, $i = 3, \ldots, n$ are functions of the control parameters S,L. As usual, the expansion is cut at order $n > 3$, with A_n being the first non-negative coefficient. The powers appearing in the expansion are dictated by the symmetry of the system; for cylindrically symmetric geometries, only even powers are allowed. In the following sections, we will reobtain these results in an analytical fashion for certain simple geometries of the substrate.

III. DETACHMENT DUE TO OUT-OF-PLANE MODES FOR RADIAL SYMMETRY

As we stated in Sec. II, for 1D geometries the solution obtained by only considering the bending rigidity term in the elastic free energy is exact. For three-dimensional (3D) geometries, this is an approximation that works well for small height fluctuations of the substrate. Our aim in this section is to obtain analytical results in this limit to achieve a qualitative understanding of the depinning process. Analytical results can be obtained for certain simple geometries; we will restrict our analysis to cylindrically symmetric cases. We consider first a substrate with an axially symmetric *depression* $s(r)$ as shown in Fig. 3. The biharmonic equation (7) in cylindrical coordinates, assuming a rotational invariant case, is given by

$$\left(\frac{1}{r}\partial_r + \partial_r^2\right)^2 h(r) = 0, \quad (19)$$

which has the following general solution:

$$h(r) = H_0 + H_1 \log r + \frac{H_2}{2}r^2 + H_3 r^2 \log r. \quad (20)$$

For a depression, if we assume that the membrane detaches from the substrate homogeneously at a circumference of radius R (to be determined), the solution Eq. (20) is valid for $0 \leqslant r \leqslant R$ and hence it has to be regular at the origin, $H_1 = H_3 = 0$. The radius $r = R$ gives the parametrization of the curve of

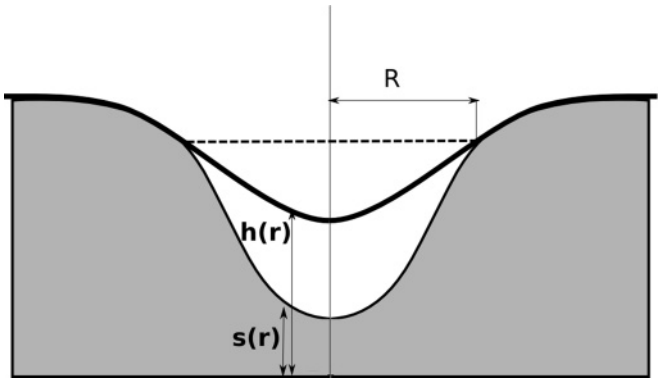

FIG. 3. Membrane on top of a substrate with a depression. The figure is axially symmetric with respect to the vertical axis through the center of the substrate's depression. R indicates the radius of detachment. The dashed line represents the approximation used in Sec. IV for when the in-plane modes are taken into account.

detachment $\mathbf{x}^*$ introduced in Sec. II. The boundary conditions Eqs. (8)–(10) take the form

$$\begin{aligned} h(R) &= s(R), \\ h'(R) &= s'(R), \\ \frac{h'(R)}{R} + h''(R) &= \frac{s'(R)}{R} + s''(R) \pm \sqrt{\frac{\gamma_S}{\kappa}}. \end{aligned} \tag{21}$$

Applying the boundary conditions Eq. (21) over the general solution Eq. (20), we obtain

$$\begin{aligned} h(r) &= s(R) - \frac{s'(R)}{2}R + \frac{s'(R)}{2R}r^2, \\ \frac{s'(R)}{R} &= s''(R) \pm \sqrt{\frac{\gamma_S}{\kappa}}. \end{aligned} \tag{22}$$

The second equation determines the radius of detachment, but also imposes a condition over the substrate profile for a nontrivial solution to exist (note that there is always a solution with $R = 0$). As we pointed out in Sec. II, the radius of detachment R corresponds to extrema of the total energy of the membrane, which within the present approximation consists of

$$E_{\mathrm{BD}}^{\mathrm{Tot}}(R) = E_{\mathrm{pin}}(R) + E_{\kappa}(R), \tag{23}$$

with E_{pin} the pinning energy and E_{κ} the bending energy. In cylindrical coordinates, these are given, respectively, by

$$E_{\mathrm{pin}}(R) \approx \gamma_S \int_0^R \pi r dr, \tag{24}$$

$$\begin{aligned} E_{\kappa}(R) = \pi\kappa \int_0^R r dr \left[\left(\frac{1}{r}\partial_r + \partial_r^2\right)h(r)\right]^2 \\ - \pi\kappa \int_0^R r dr \left[\left(\frac{1}{r}\partial_r + \partial_r^2\right)s(r)\right]^2. \end{aligned} \tag{25}$$

In both of these expressions, the energy is measured from the totally pinned configuration. The total energy $E_{\mathrm{BD}}^{\mathrm{Tot}}(R)$ allows us to determine the stability of the solutions $R = 0$ and Eq. (22). This is simply exemplified for the case of a parabolic well.

A. Parabolic well

In the case of a parabolic profile $s(r) = S_0 + \frac{S_2}{2}r^2$, we see that (22) implies that $h(r) \equiv s(r)$ and there is no solution for a partially detached membrane. If we allow for a quartic term $s(r) = S_0 + \frac{S_2}{2}r^2 + \frac{S_4}{24}r^4$, then we obtain that the detachment radius is given by

$$R_*^2 = \frac{3}{S_4}\sqrt{\frac{\gamma_S}{\kappa}}, \tag{26}$$

where we have taken the minus sign in the second equation of (22) corresponding to the fact that the curvature of the detached membrane is smaller than that of the substrate. Therefore, S_4 needs to be a positive quantity for a solution to exist. From the total energy $E_{\mathrm{BD}}^{\mathrm{Tot}}(R)$ given by Eq. (23), it is easy to show that the solution given by Eq. (26) corresponds to a maximum of the energy profile, and hence it is an unstable equilibrium solution while $R = 0$ is a metastable minimum. $E_{\mathrm{BD}}^{\mathrm{Tot}}(R) \to -\infty$ for $R \to \infty$ and therefore R_* signals the energy barrier for total depinning, which is always the stable configuration. This is, however, a construction of the unbounded quartic profile we have chosen for the substrate. In the next sections, we will study in detail a more physically sensible profile: a Gaussian depression or protrusion.

B. Gaussian depression

A more realistic landscape for the substrate is the case of a Gaussian depression,

$$s(r) = G_s\left(1 - e^{-\frac{r^2}{2\sigma^2}}\right). \tag{27}$$

For this geometry, the curvature of the substrate varies from positive to negative along the radial coordinate, and therefore we have to allow for both signs $\pm\sqrt{\frac{\gamma_S}{\kappa}}$ in Eq. (22). However, when the condition is applied to this particular shape, we obtain

$$\frac{s'(R)}{R} - s''(R) = \frac{G_s}{\sigma^2}\frac{R^2}{\sigma^2}e^{-\frac{R^2}{2\sigma^2}} = \sqrt{\frac{\gamma_S}{\kappa}}, \tag{28}$$

that is, only the positive sign leads to the existence of a solution since we have assumed $G_s > 0$. The solution for the membrane's profile is then given by

$$h(r) = \begin{cases} G_s - G_s e^{-\frac{R^2}{2\sigma^2}}\left(1 + \frac{R^2 - r^2}{2\sigma^2}\right), & 0 \leqslant r \leqslant R \\ s(r), & r > R, \end{cases} \tag{29}$$

with R given by (28).

We apply this solution now to the particular case of graphene on top of a SiO_2 substrate. As we did in Eq. (17), in what follows we will treat all length quantities as dimensionless, given in units of the characteristic length ℓ defined in Eq. (5). We can consider, as an example to illustrate the solutions given by Eqs. (28) and (29), a particular substrate depression of amplitude $G_s = 1$ and width $\sigma = 2$. We obtain two possible solutions for a partially detached configuration: $R_1 \approx 0.45$ and $R_2 \approx 2.75$. In Fig. 4, we depict the graphene membrane profile solutions that correspond to this particular configuration.

To study the stability of the obtained solutions, we use the total energy, which, by Eq. (23), is given by [for the figures,

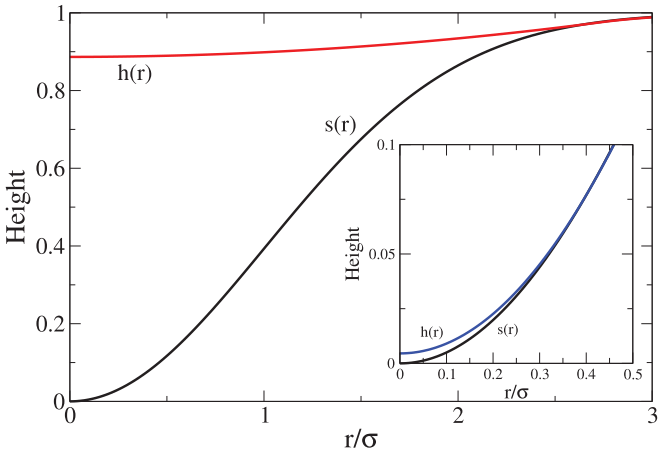

FIG. 4. (Color online) Graphene depinning from a Gaussian depression in the BD regime. The plots show the profile of the graphene membrane $h(r)$ (color) and of the substrate $s(r)$ (black), in units of ℓ, as a function of the distance from the center of the depression in units of the depression characteristic width σ. The figures have axial symmetry. Main figure: stable solution with the graphene sheet almost completely detached ($R_2 \approx 5.5$). Inset: Unstable solution with very little detachment of the graphene sheet ($R_1 \approx 0.9$). Height profile as a function of the radial distance to the center of the depression, r. We have taken $G_s = 1$ and $\sigma = 2$. All quantities are in units of the characteristic length $\ell \approx 1$ Å.

we have used the exact expression for the pinning energy, $E_{\rm pin} = -\gamma\pi \int r dr \sqrt{1 + \left(\frac{G_s}{\sigma^2} r e^{-\frac{r^2}{2\sigma^2}}\right)^2}]$

$$E^{\rm Tot}_{\rm BD}(R) = \sigma^2 \left\{ \frac{\gamma_S \pi R^2}{2\sigma^2} + \frac{G_s^2}{\sigma^4}\kappa\pi \times \left[e^{-\frac{R^2}{\sigma^2}} \left(\frac{1}{2}\frac{R^4}{\sigma^4} + \frac{R^2}{\sigma^2} + 1 \right) - 1 \right] \right\}. \quad (30)$$

The total energy $E^{\rm Tot}_{\rm BD}(R)$ corresponding to the substrate profile shown in Fig. 4 is given in Fig. 5 as a function of the detachment radius R. We see that the completely pinned situation ($R_0 = 0$) is a metastable state with a very small energy barrier to overcome to reach the true minimum R_2. The solution R_1 corresponds to a maximum of the energy, and hence it is an unstable configuration.

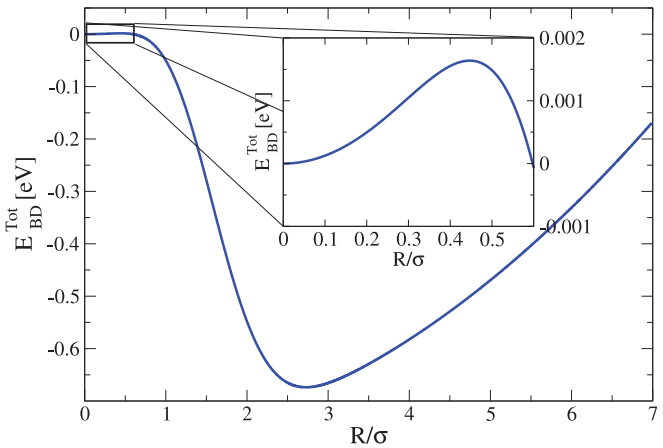

FIG. 5. (Color online) Main figure: Total energy as a function of the detachment radius R in units of the characteristic width σ, for a Gaussian depression in the bending rigidity dominated regime. Inset: Closeup showing the metastable solution at $R_0 = 0$ and the unstable solution R_1. Results for $G_s = 1$ and $\sigma = 2$.

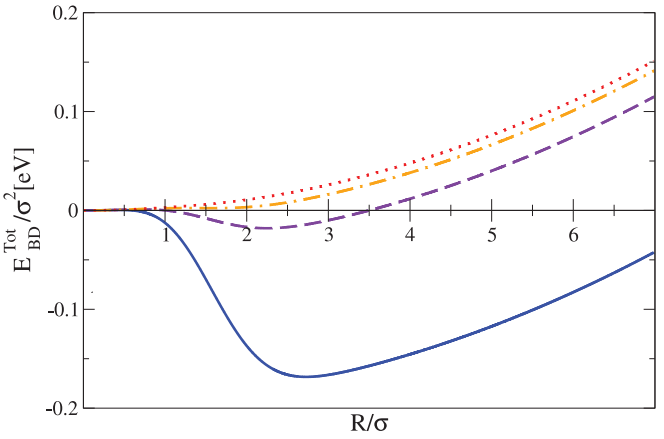

FIG. 6. (Color online) Energy landscape as a function of detachment radius in the bending rigidity dominated regime for a Gaussian depression with varying $\frac{G_s}{\sigma^2}$. Solid (blue): $\frac{G_s}{\sigma^2}\big|_1 = 0.25$; dashed (purple): $\frac{G_s}{\sigma^2}\big|_2 \approx 0.08$; dash-dot (orange): $\frac{G_s}{\sigma^2}\big|_3 \approx 0.06$; dotted (red): $\frac{G_s}{\sigma^2}\big|_4 \approx 0.03$. The energy presents a minimum for the detached configuration for cases 1, 2, and 3 (this last one being metastable), while for case 4 the energy is a minimum only for the completely pinned configuration, in agreement with the threshold value discussed in the main text. For cases 1, 2, and 3, the completely pinned configuration is a local minimum with a low-energy barrier, not visible due to the large scale of the plot. Note that σ and G_s are dimensionless: $\sigma, G_s \to \sigma/\ell, G_s/\ell$.

By rescaling the radius of detachment R by the depression width σ, $\tilde{R} = R/\sigma$, the rescaled energy $E^{\rm Tot}_{\rm BD}(\tilde{R})/\sigma^2$ depends only on the ratio G_s/σ^2, and hence the results can be expressed in an universal manner. In Fig. 6, we show the rescaled energy $E^{\rm Tot}_{\rm BD}(\tilde{R})/\sigma^2$ landscape for various values of G_s/σ^2. As expected, the global minimum corresponding to the partially detached configuration evolves into a metastable state as G_s/σ^2 is decreased, and disappears completely for small enough G_s/σ^2. As discussed in Sec. II, the threshold value for a stable pinned configuration given by Eq. (17) is $G_s/\sigma^2 = \ell\sqrt{\frac{\gamma_S}{\kappa}} \approx 0.05$. As can be seen from the figure, this estimated threshold is in excellent agreement with the exact results.

In Sec. II, we stated that the length of the detachment curve $|\mathbf{x}^*|$ is the natural order parameter that controls the pinned-to-depinned phase transition of the system. This can be easily seen now from Fig. 6. Given the cylindrical geometry of the problem, the length of the curve $\mathbf{x}^*$ is given by $|\mathbf{x}^*| = 2\pi R\ell$, and hence we can take R as our order parameter. As discussed, from Fig. 6 we see that the minimum at finite R evolves into a metastable state that disappears for shallow enough depressions, while $R = 0$ is the true minimum in this case, indicating that the transition is a first-order one. This can be seen in an alternative way by following the evolution of the order parameter R. From Eq. (29) again we note that $\tilde{R}$ is controlled solely by the ratio G_s/σ^2, in agreement with Eq. (17) and with the universal form of the rescaled energy

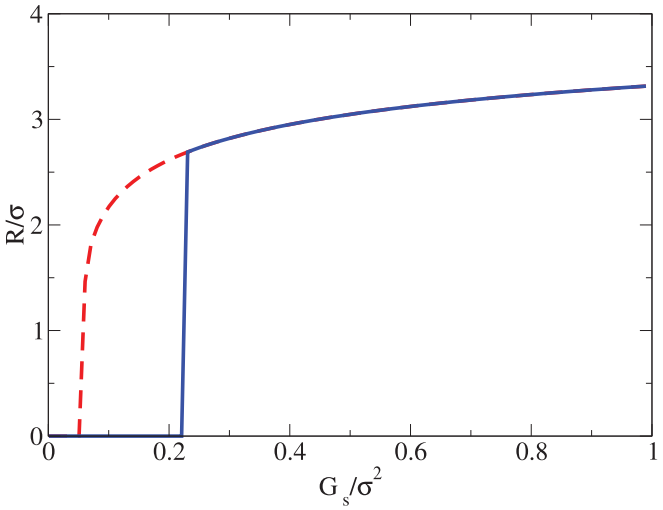

FIG. 7. (Color online) Order parameter $\tilde{R} = R/\sigma$ as a function of the ratio G_s/σ^2 of a Gaussian depression in the BD regime. The dashed (red) line indicates the spinodal line, while the solid (blue) line corresponds to the true transition.

$E^{\rm Tot}_{\rm BD}(\tilde{R})/\sigma^2$. The behavior of $\tilde{R}$ as a function of G_s/σ^2 is shown in Fig. 7, where we see that $\tilde{R}$ jumps from $\tilde{R} = 0$ to a finite value at a critical value $G_s/\sigma^2|_c \approx 0.2$. The figure also shows the spinodal point, that is, the value $G_s/\sigma^2|_s \approx 0.05$ at which the first metastable solution appears, in agreement with the estimated threshold value. The difference between $G_s/\sigma^2|_c$ and $G_s/\sigma^2\big|_s$ shows that the system in the BD regime limit is strongly hysteretic. The critical point $G_s/\sigma^2|_c$ and the spinodal point $G_s/\sigma^2\big|_s$ can be estimated from an expansion of the free energy Eq. (30) in the rescaled order parameter $\tilde{R}$:

$$\frac{E^{\rm Tot}_{\rm BD}}{\sigma^2} \approx \frac{\pi}{2}\left[\gamma_S \tilde{R}^2 + \kappa\left(\frac{G_s}{\sigma^2}\right)^2\left(-\frac{\tilde{R}^6}{3} + \frac{\tilde{R}^8}{4}\right)\right]. \quad (31)$$

This expansion can be identified with the Landau expansion Eq. (18), and it assumes that the rescaled order parameter $\tilde{R}$ is small, and hence (assuming a weak first-order transition) it is valid near the critical point $G_s/\sigma^2|_c$. By minimizing Eq. (31), it is easy to see that the condition for the existence of metastable solutions with $\tilde{R} \neq 0$ is given by $(G_s/\sigma^2)^2 \gtrsim (27/4)\gamma_S \approx 0.12$, a value that is of the order of magnitude of the spinodal point obtained exactly in Fig. 7. For $(G_s/\sigma^2)^2 (\gtrsim 27/4)\gamma_S$, the extrema condition $dE^{\rm Tot}_{\rm BD}/d\tilde{R} = 0$ in expression Eq. (31) renders $\tilde{R}_0 = 0$ plus two real positive roots in agreement with the energy profiles presented in Fig. 6 for the exact solution Eq. (30).

C. Gaussian bump

For a Gaussian *protrusion*

$$s(r) = G_s e^{-\frac{r^2}{2\sigma^2}}, \quad (32)$$

the general solution Eq. (20) holds for $r > R$. Since the origin is avoided, H_1 and H_3 can be different from zero. This solution, however, diverges for $r \to \infty$ unless $h(r) = \text{const}$, which in turn cannot satisfy $h'(R) = s'(R)$. Hence a kind of solution for which the graphene membrane follows the substrate for $0 < R < r$ and then detaches "forever" is not possible. The most general solution is to assume that there is a radius of detachment R and a radius of reattachment L, with $R < L$. The gain in pinning and bending energies with respect to the totally attached configuration in this case are given by

$$E_{\rm pin}(R) \approx \gamma_S \int_R^L \pi r dr, \quad (33)$$

$$E_\kappa(R) = \pi\kappa \int_R^L r dr\left[\left(\frac{1}{r}\partial_r + \partial_r^2\right)h(r)\right]^2 - \pi\kappa \int_R^L r dr\left[\left(\frac{1}{r}\partial_r + \partial_r^2\right)s(r)\right]^2. \quad (34)$$

Intuitively, it is easy to see that if the bump is very pronounced, R has to be approximately zero, otherwise the bending-energy cost is too high. A sketch of the system is shown in Fig. 8. Assuming this type of configuration, the general solution Eq. (20) holds now for $0 \leqslant r \leqslant L$, with $H_1 = 0$ for it to be regular at the origin. The constant H_3 in this case is allowed to be finite since the contact force is acting at $r = 0$.[23] Imposing continuity of the solution and its first derivative at $r = L$, and $h(0) = s(0)$ [note that $h(r) \to H_0$ for $r \to 0$], for the region $0 \leqslant r \leqslant L$ we obtain for the membrane profile

$$h(r) = G_s - \frac{G_s}{L^2}e^{-\frac{L^2}{2\sigma^2}}\left[-1 + e^{\frac{L^2}{2\sigma^2}} - \frac{L^2}{2\sigma^2}\log(L^2) - \log(L^2) + !e^{\frac{L^2}{2\sigma^2}}\log(L^2)\right]r^2 + \frac{G_s}{L^2}e^{-\frac{L^2}{2\sigma^2}}\left[-\frac{L^2}{2\sigma^2} - 1 + e^{\frac{L^2}{2\sigma^2}}\right] \times r^2\log(r^2), \quad (35)$$

while $h(r) = s(r)$ for $r > L$. The optimal value of L can be obtained numerically, as previously, by imposing the discontinuity of the Laplacian of the solution due to the contact force. However, since we are interested in the qualitative aspect of the solution, it is simpler to analyze directly the energy profile as a function of the reattachment radius L. As was the case for the Gaussian depression in Sec. III B, the energy Eq. (35) and the reattachment radius L can be rescaled by the

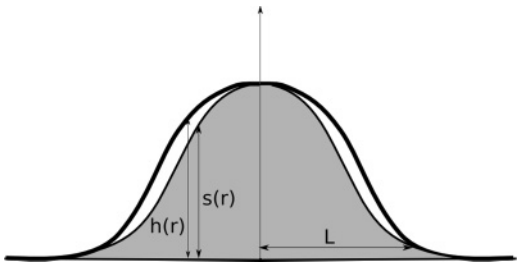

FIG. 8. Membrane on top of a substrate with a protrusion. The figure is axially symmetric with respect to the vertical axis through the center of the substrate's bump. As discussed in the text, the membrane is shown as depinning from the top of the bump, and reattaching at a radius L.

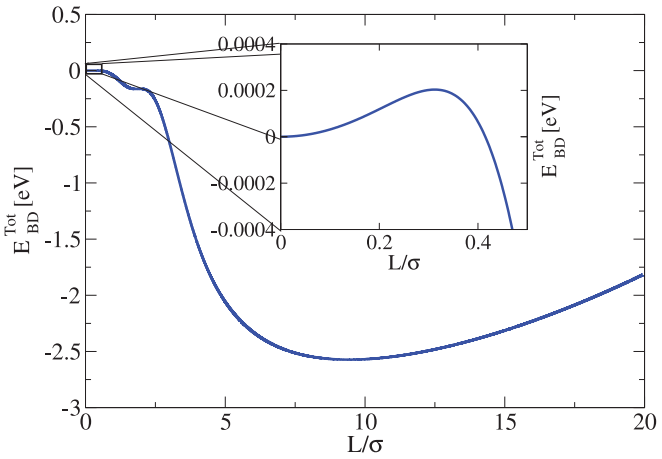

FIG. 9. (Color online) Main figure: Total energy as a function of the reattachment radius L for a pronounced Gaussian bump in the bending rigidity dominated regime. Inset: Closeup near the metastable configuration corresponding to a completely pinned membrane. We have taken $G_s = 1$ and $\sigma = 2$.

width of the bump to show the universal behavior,

$$\frac{E_{\rm BD}^{\rm Tot}(\tilde{L})}{\sigma^2} = \gamma_S \pi \frac{\tilde{L}^2}{2} + \kappa\pi \frac{G_s^2}{2\sigma^4} e^{-\tilde{L}^2}\left[\tilde{L}^4 + 6\tilde{L}^2 + 2\left(9 - 8e^{-\frac{\tilde{L}^2}{2}}\right) - 16\left(1 - e^{-\frac{\tilde{L}^2}{2}}\right)^2 \frac{1}{\tilde{L}^2}\right] - \kappa\pi \frac{G_s^2}{2\sigma^4}, \tag{36}$$

with $\tilde{L} = L/\sigma$. The energy profile Eq. (36) is shown in Fig. 9 for a bump with $G_s = 1$ and $\sigma = 2$, as a function of the reattachment radius $\tilde{L}$. From the figure, it can be seen that the case of total adhesion of the graphene membrane to the substrate, in the case of a pronounced bump, is a metastable state with a very low energy barrier to fall into a configuration for which the membrane attaches to the substrate after a finite radius L.

As we mentioned previously, the solution Eq. (35) is valid in principle for pronounced Gaussian protrusions, for which $G_s/\sigma^2 \gtrsim 1$. However, it can be shown that this is true for any Gaussian bump. This can be seen more rigorously by calculating the most general solution for which both the depinning and reattachment radius are finite, and finding the minimum of the energy surface. The explicit solution for this most general case is rather cumbersome, and it is given in Appendix A. Here we show a plot of the energy surface profile as a function of both detachment and reattachment radius $\tilde{R}$ and $\tilde{L}$. As can be seen from Figure 10, the complete solution indeed shows that the case $R = 0$ and finite L is a minimum for the case $G_s/\sigma^2 = 1$, and the same can be shown for other aspect ratio protrusions. From Eq. (36) it is evident that $E_{\rm BD}^{\rm Tot}(L/\sigma)/\sigma^2$ depends only on the ratio G_s/σ^2. The rescaled energy profile projection onto the $R = 0$ plane, $E_{\rm BD}^{\rm Tot}(\tilde{L})/s^2$, for varying G_s/σ^2 is shown in Fig. 11, showing the crossover from the pinned to the partially detached configuration for increasingly pronounced bumps. As in the case of a Gaussian depression analyzed in the previous subsection, the case of a finite reattachment radius $\tilde{L}$ is the energy minimum for $G_s/\sigma^2 \gtrsim 0.05$, while in the opposite limit the minimum corresponds to $L = 0$, that is, for smooth bumps the membrane minimizes its energy by conforming completely to the substrate.

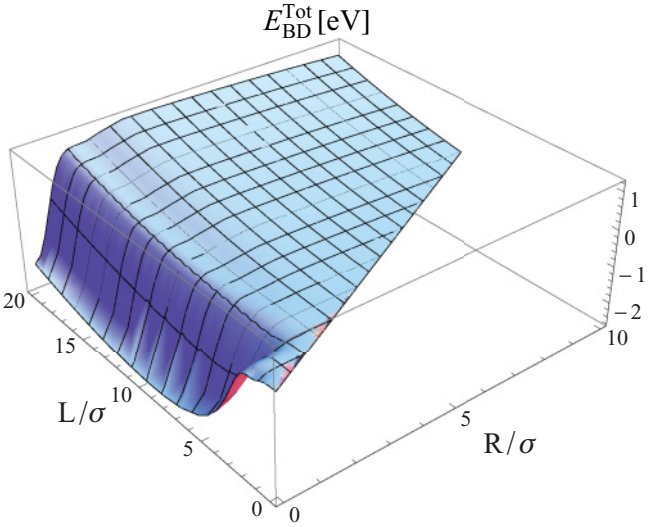

FIG. 10. (Color online) Energy profile as a function of detachment radius $\tilde{R} = R/\sigma$ and reattachment radius $\tilde{L} = L/\sigma$ with $G_s/\sigma^2 = 1$ for a Gaussian bump. The global minimum corresponds to $\tilde{R} = 0$ and finite $\tilde{L}$.

Similar results to those obtained in Sec. III B for the behavior of the rescaled order parameter $\tilde{R}$ as a function of G_s/σ^2 can be obtained here for $\tilde{L}$, showing a first-order phase transition between the pinned and depinned phases.

IV. DETACHMENT DUE TO IN-PLANE MODES FOR RADIAL SYMMETRY

In the previous sections, we studied the detachment of a graphene membrane from a patterned substrate due to the bending rigidity term in the free energy Eq. (2). This approximation is widely used, but, as we showed, it is valid

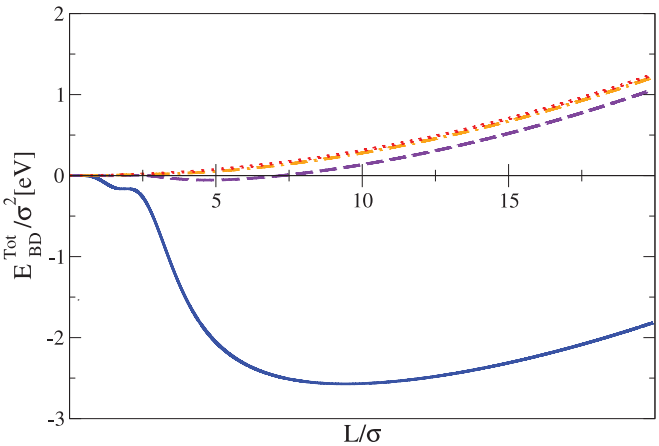

FIG. 11. (Color online) Energy landscape as a function of reattachment radius $\tilde{L} = L/\sigma$ in the BD regime for a Gaussian protuberance of varying ratio $\frac{G_s}{\sigma^2}$. Solid (blue): $\frac{G_s}{\sigma^2}\big|_1 = 1$; dashed (purple): $\frac{G_s}{\sigma^2}\big|_2 = 0.25$; dash-dot (orange): $\frac{G_s}{\sigma^2} \approx 0.1\big|_3$; dotted (red): $\frac{G_s}{\sigma^2} \approx 0.04\big|_4$. The energy presents a minimum for the partially detached configuration for case 1 that disappears completely for case 4, going through a metastable state for case 3. Note that σ is dimensionless: $\sigma \to \sigma/\ell$.

for relatively small fluctuations of the substrate landscape for a 3D pattern. In this section, we consider the less studied case of depinning due to in-plane modes, for which the free energy Eq. (1) is approximated by Eq. (14). As before, we will restrict our study to cases that allow for an analytic solution, in particular a substrate with radial symmetry. In cylindrical coordinates, this elastic energy is given by

$$E_{\rm el} = \frac{\lambda}{2}\int 2\pi r dr\left[\partial_r u_r + \frac{u_r}{r} + \frac{1}{2}(\partial_r h)^2\right]^2 + \mu\int 2\pi r dr\left[\partial_r u_r + \frac{1}{2}(\partial_r h)^2\right]^2 + \mu\int 2\pi r dr\left(\frac{u_r}{r}\right)^2, \tag{37}$$

where u_r is the radial component of the in-plane displacements, and $E_{\rm pin}$ was defined in (24). In the following subsections, we will obtain results for a Gaussian depression and protrusion.

A. Gaussian depression

In this subsection, we consider again a Gaussian depression given by Eq. (27), over which there is a membrane partially attached. For radius greater than a radius R, the membrane is pinned to the substrate and follows its profile, while for $0 < r < R$ the membrane is completely detached. When analyzing the effect of the in-plane modes, we encounter an added complication: we do not know the height profile of the membrane for the detached region, since this would imply solving the problem completely by treating the full coupled nonlinear differential equations in both h and $\mathbf{u}$ fields resulting from minimizing Eq. (1). Here we consider as a first approximation that the graphene membrane remains flat within the detached region, as shown in Fig. 3. Hence the differential equation to solve is given by

$$-(\lambda+2\mu)\left(\partial_r^2 u_r + \frac{\partial_r u_r}{r} - \frac{u_r}{r^2}\right) = \begin{cases} 0, & 0 \leqslant r \leqslant R \\ (\lambda+2\mu)\partial_r s\left(\partial_r^2 s\right) + \frac{\mu}{r}(\partial_r s)^2, & r > R. \end{cases} \tag{38}$$

Our ansatz corresponds to a membrane profile given by

$$h(r) = \begin{cases} h_0, & 0 \leqslant r \leqslant R \\ s(r), & r > R \end{cases} \tag{39}$$

with $s(r)$ given by Eq. (27). The general solution of Eq. (38) is given by (see Appendix B)

$$u_r(r) = \begin{cases} r\frac{G_s^2}{4\sigma^2}\frac{\mu}{(\lambda+2\mu)}e^{-\frac{R^2}{\sigma^2}}, & 0 \leqslant r \leqslant R \\ \frac{G_s^2}{4}e^{-\frac{r^2}{2\sigma^2}}\left[\frac{r}{\sigma^2} + \frac{(\lambda+\mu)}{(\lambda+2\mu)}\frac{1}{r}\right] - \frac{1}{r}\frac{G_s^2}{4\sigma^2}\frac{(\lambda+\mu)}{(\lambda+2\mu)}(R^2+\sigma^2)e^{-\frac{R^2}{\sigma^2}}, & r > R. \end{cases} \tag{40}$$

The radius R of detachment can be found by finding the extrema of the total energy $E_{\rm SD}^{\rm Tot}(R) = E_{\rm pin}(R) + E_{\rm el}(R)$, where $E_{\rm pin}$ is given by Eq. (24) and we measure the elastic energy Eq. (37) from the totally attached configuration. The total energy as a function of detachment radius can be calculated to be

$$E_{\rm SD}^{\rm Tot}(R) = \sigma^2\frac{\pi}{2}\left\{\gamma_S\frac{2R^2}{\sigma^2} + \frac{G_s^4}{\sigma^4}\frac{\mu(\lambda+\mu)\pi}{8(\lambda+2\mu)}\left[e^{-\frac{2R^2}{\sigma^2}}\left(2\frac{R^2}{\sigma^2}+1\right)-1\right]\right\}. \tag{41}$$

Minimizing $E_{\rm SD}^{\rm Tot}(R)$ renders a solution with $R_0 = 0$, which is a local minimum and corresponds to the membrane completely pinned, and the following transcendental equation for the equilibrium detachment radius:

$$\gamma_S = \frac{G_s^4}{2\sigma^4}\frac{R^2}{\sigma^2}\mu^2\frac{(\lambda+\mu)}{(\lambda+2\mu)^2}e^{-\frac{2R^2}{\sigma^2}}. \tag{42}$$

Again, as in the BD dominated regime case of Sec. III, we see that by rescaling both the detachment radius and the total energy by an overall factor given by the depression width σ, $\tilde{R} = R/\sigma$, and $E_{\rm SD}^{\rm Tot}(\tilde{R})/\sigma^2$, the rescaled energy shows universality. In this case, and in agreement with Eq. (17), the system is controlled by the ratio G_s/σ, contrary to the dependence on G_s/σ^2 found for the BD regime.

We can apply our results to a graphene membrane on top of a SiO_2 substrate as we did in Sec. III. Taking the accepted values for room temperature for the Lamé coefficients of graphene, $\mu \approx 10$ eV Å^{-2}, $\lambda \approx 2$ eV Å^{-2},[19] and $G_s = 5$ (in accordance with the validity of our approximation), as well as $\sigma = 4$ (note that we are still working in units of the scaling length ℓ), we get two possible depinning radii: $R_1 \approx 0.1$ corresponding to an unstable minimally detached configuration, and $R_2 \approx 8.4$, which is the stable, global minimum solution. The total energy $E_{\rm SD}^{\rm Tot}$ is plotted as a function of detachment radius $\tilde{R} = R/\sigma$ in Fig. 12, showing the different equilibrium solutions. The energy barrier to be overcome for detachment from the metastable equilibrium configuration at $R_0 = 0$ is very small, as can be seen from the inset in Fig. 12. Note also that the minimum at R_2 is very shallow in comparison to the energy scale, as shown in the inset of Fig. 12, and hence any fluctuation could lead to the graphene membrane being detached at a radius $R > R_2$, and therefore closer to the flat configuration. This effect is less pronounced as the width of the depression is increased.

In Section II, Eq. (17), for the SD regime we predicted a critical value for the ratio G_s/σ above which the stable configuration is that of the membrane partially detached from the substrate. Taking the values for graphene discussed above, this ratio is given by $(4\frac{\gamma_S}{E_{2D}})^{1/4} \approx 0.1$. This estimate is in good

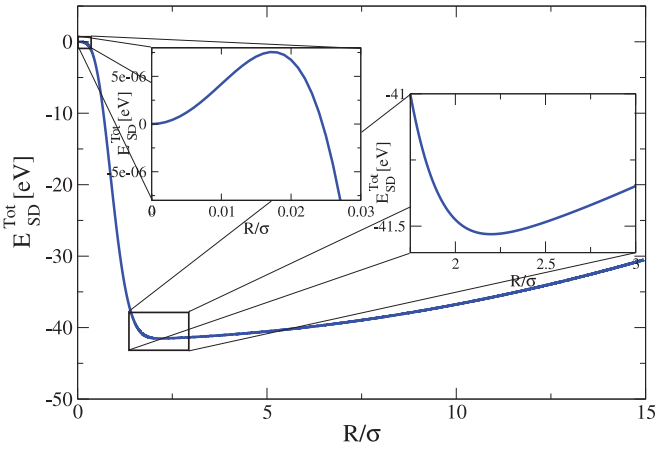

FIG. 12. (Color online) Energy profile for a Gaussian depression as a function of detachment radius $\tilde{R} = R/\sigma$ for $G_s = 5$ and $\sigma = 4$, as discussed in the main text. The insets show the local minimum that corresponds to the totally pinned configuration and the global minimum corresponding to the partially detached membrane.

agreement with the exact results for the rescaled energy profile $E_{\rm SD}^{\rm Tot}(\tilde{R})/\sigma^2$ depicted in Fig. 13, as a function of the rescaled detachment radius $\tilde{R}$ and varying G_s/σ.

As discussed in Sec. III, the radius of detachment R can be taken as the order parameter of the problem. We show the behavior of $\tilde{R} = R/\sigma$ as a function of G_s/σ in Fig. 14. Again, a pronounced jump in $\tilde{R}$ to a finite value with increasing G_s/σ is observed at a critical value $G_s/\sigma|_c$, in agreement with the predicted threshold for the transition. The spinodal line, also shown in Fig. 14, is basically indistinguishable from the true

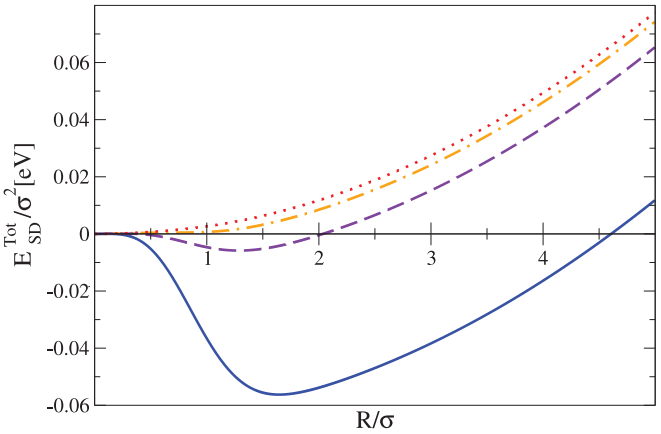

FIG. 13. (Color online) Energy landscape in the SD regime as a function of detachment radius $\tilde{R} = R/\sigma$ for a Gaussian depression of varying ratio $\frac{G_s}{\sigma}$. Solid (blue): $\frac{G_s}{\sigma}\big|_1 = 0.5$; dashed (purple): $\frac{G_s}{\sigma}\big|_2 \approx 0.33$); dash-dot (orange): $\frac{G_s}{\sigma}\big|_3 = 0.25$; dotted (red): $\frac{G_s}{\sigma}\big|_4 \approx 0.17$. The energy presents a minimum for the detached configuration for cases 1, 2, and 3 (this last one being metastable), while for case 4 the energy is a minimum only for the completely pinned configuration, in agreement with the threshold value discussed in the main text. For cases 1 and 2, the completely pinned configuration is a local minimum with a low-energy barrier, not visible due to the large scale of the plot. The region of metastability for the depinned configuration is very small, as seen in this plot and also in Fig. 14. Note that σ is dimensionless: $\sigma \to \sigma/\ell$.

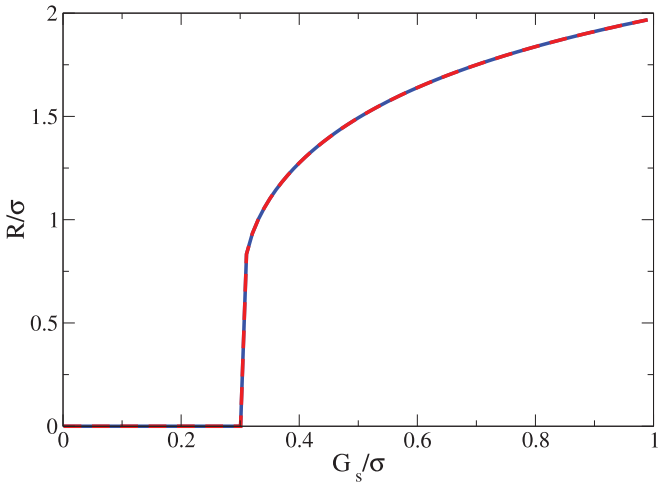

FIG. 14. (Color online) Order parameter R as a function of height G_s of the Gaussian depression in units of σ in the SD regime. The dashed (red) line indicates the spinodal line, while the solid (blue) line corresponds to the true transition. In the SD regime, these two lines are indistinguishable.

transition, and hence in the SD regime there is almost no hysteresis.

The expansion of the free energy Eq. (41) in powers of the order parameter $\tilde{R}$,

$$\frac{E_{\rm SD}^{\rm Tot}(\tilde{R})}{\sigma^2} \approx \frac{\pi}{2}\left\{\gamma_S \tilde{R}^2 + \frac{G_s^4}{\sigma^4}\frac{\mu(\lambda+\mu)}{(\lambda+2\mu)}\left[-\frac{\tilde{R}^4}{4} + \frac{\tilde{R}^6}{3}\right]\right\}, \tag{43}$$

gives a good qualitative description of the first-order transition obtained exactly in Fig. 14. Moreover, in this case the spinodal point given by the expansion Eq. (39) is given by $(G_s/\sigma)^4 = (44/15)\gamma_S$, giving $G_s/\sigma|_s \approx 0.28$, in excellent numerical agreement with the exact value.

B. Gaussian bump

Following similar manipulations to the previous section, we can calculate the solution for the radial component for the in-plane displacements in the graphene membrane due to a Gaussian protrusion parametrized by Eq. (32). Given our findings for the BD regime in Sec. III C, we consider a configuration of the membrane on top of the substrate that is pinned at the very top (detachment radius $R = 0$) and reattaches at a radius L as shown in Fig. 8. This takes into account the energetic cost of bending. As in Sec. III B, we have to make a sensible approximation for the unknown profile of the membrane on the detached section. Hence we hence approximate the detached profile of the membrane by the general solution valid for small protrusions (BD regime), Eq. (20).[24] The details for the solution using this ansatz are given in Appendix B. Imposing the boundary conditions results in two possible solutions, leading to the two energy profiles shown in Fig. 15 for $G_s = 5$ and $\sigma = 4$. Although these solutions differ for the metastable or unstable regions (a construction of the approximation involved), they coincide for the minimum, and hence the stable reattachment radius L is uniquely defined.

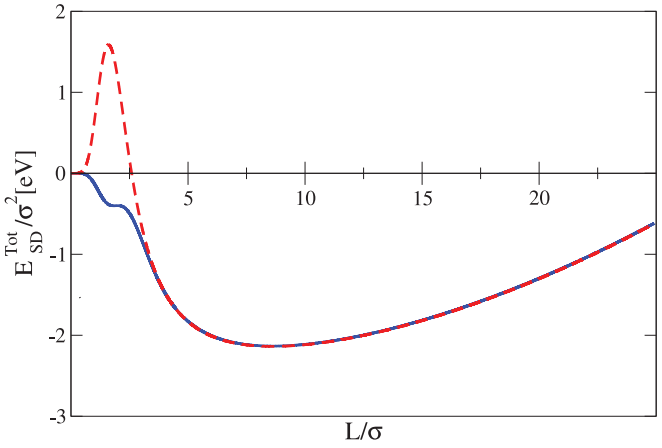

FIG. 15. (Color online) The two possible solutions for the energy profile as a function of re-attachment radius $\tilde{L} = L/\sigma$ in the SD regime, as calculated in Appendix B. We have taken $G_s = 5$ and $\sigma = 4$.

V. DISCUSSION

In this work, we have analyzed the possibility of depinning of a membrane on top of a patterned substrate. We have studied simple configurations of the substrate that allow for analytical solutions in the two relevant limits for the problem: the bending rigidity dominated regime, valid for small corrugations of the substrate, and the elastic, strain dominated regime, which holds for larger corrugations. We have shown that in both limits, the energy cost of either bending or stretching can cause the membrane to prefer to detach from the substrate. The particular results confirm the more general picture we sketched in Sec. II, in which we obtained a qualitative phase diagram for the system presented in Fig. 2. This phase diagram presents two phases: a completely pinned phase in which the membrane follows the profile of the substrate, and a detached phase in which the membrane prefers to depin partially at some optimal detachment curve $\mathbf{x}^*$. We have shown that an order parameter can be constructed from this detachment curve, which allows us to write the problem in terms of a Landau energy functional Eq. (18). By scaling arguments, we were also able to obtain the critical lines (17) in both BD and SD limiting regimes, and we found excellent agreement with analytical calculations. The critical line in Fig. 2 represents a first-order phase transition, as argued in Sec. II and shown explicitly for specific geometries of the substrate. We showed that the energy of the system shows universality, and depends on the ratio of S/L or S/L^2 for the SD and BD regimes, where S is the height of the substrate's corrugation and L is its characteristic width. We obtained the critical and spinodal points exactly for the analytically solvable cases, and we showed that the Landau energy functional gives a very good estimate to locate these points.

The depinning process is dependent on the aspect ratio of the spatial perturbations of the substrate, the elastic parameters of the membrane, and its interaction with the substrate. The interaction between graphene and different types of substrates is not well known. Order-of-magnitude estimates for different mechanisms[17] suggest that the interaction coupling $\gamma_S \sim 10^{-2} - 2$ meV Å^{-2} [note that the interaction between two graphene layers in graphite is 20–30 meV Å^{-2} (Ref. 17)]. Within this work, we have set $\gamma_S = 2$ meV Å^{-2}, its most conservative value, and hence the obtained values for depinned configurations are underestimations. For this value of γ_S, we find that, in the elastic regime, the depinning of graphene becomes relevant for height corrugations such that $S/L \gtrsim 1/10$. In the bending regime, the condition depends on the total area of the corrugation: $S/L^2 \gtrsim 1/20$ Å^{-1}. These obtained values for possible depinning are comparable to measured corrugations in free-standing graphene[9] and in graphene on SiO_2.[11,12] Hence, regions where graphene is detached from the substrate may be found in samples on SiO_2, in agreement with the observations reported in Ref. 13. Although these conditions were obtained for the two limiting regimes, in real life both effects are present. In general, corrugations of all scales are ubiquitous due to the intrinsic roughness of the substrate, and both the bending rigidity and the in-plane strains of the graphene membrane will contribute to its depinning. Random configurations of the substrate within a mean-field model as presented in Sec. II could be treated by adding noise to the system, considering the parameters in the Landau free energy Eq. (18) as random, in the spirit of random mass theories.

The presence of corrugations in graphene, either intrinsic or substrate-induced, can lead to diverse experimental consequences. Corrugations in graphene are associated with gauge fields that couple to the Dirac electrons.[10] These gauge fields generate an effective magnetic field that can affect the transport properties of graphene. We have shown, however, that for graphene, the scale of the corrugations for which the bending rigidity is relevant is rather small. As we saw in Sec. III, the BD to SD regime crossover length for graphene is $\ell \approx 1$ Å, and hence depinning due to the strain energy cost is to be expected. The effective magnetic field is related to the strain through the relation

$$B \sim \phi_0 \frac{\beta}{a} \frac{\alpha}{L}, \tag{44}$$

where $\phi_0 \approx 10^{-15}$ Wb is the quantum of magnetic flux, $a = 1.42$ Å is the lattice parameter, and $\beta \approx 2$ gives the change in the hopping parameter between nearest sites for a Dirac electron due to the deformation of the lattice. The corrugation of the membrane determines L, the characteristic width of the corrugation, and the strain α, which for simplicity we assume to be constant. We can roughly estimate the maximum magnetic field that the graphene membrane can experience due to the corrugation of the substrate. The strain of a corrugation of height s and width L scales as s^2/L^2, and hence, from Eq. (16), the maximum strain that graphene can support is $\alpha_m \approx 2\%$. As we showed, beyond this point the membrane relaxes by depinning partially from the substrate and lowering the strain. Taking a physically relevant corrugation width of $L \approx 100$ nm, α_m corresponds to a maximum effective magnetic field of $B_m \approx 2$ T. This order of magnitude indicates that, indeed, the magnetic field due to the induced corrugations can have a sizable effect on the transport properties of graphene.[6,25] Our results indicate that rougher substrates could in fact lead to flatter configurations of the graphene membrane after annealing, due to the impossibility of graphene conforming to pronounced depressions or bumps. This could result, in a counterintuitive fashion, in greater

mobilities for graphene on top of very rough substrates, due to a decrease in impurity and phonon scattering.[7,8,26,27] On the other hand, for these kinds of substrates, the graphene membrane would be almost suspended and therefore prone to the excitation of flexural modes, which contribute to the resistivity.[28,29] A more unexplored path is the possibility of controlling the pinning or not of graphene to the substrate by tuning the different metastable states, which could be realized by modulating the gate electric field or by applying external pressure. As we showed, the system can present hysteresis and irreversibility. Our results can also be helpful to the understanding of the ubiquitous formation of graphene bubbles on many types of substrates.[30–33]

To conclude, we list the limitations of our model. Our work is based on a continuum approach and hence it breaks down for lengths of the order of the lattice spacing. However, amplitudes of the order of the lattice spacing can still be well described by the continuum model, as shown in Ref. 22. As we pointed out, the phase diagram presented in Fig. 2 is valid for 3D profiles of the substrate. The crossover to 1D geometries would, in principle, imply the disappearance of the linear critical line valid for the SD regime, since the BD results are exact for 1D. The same holds for exact calculations of Sec. III and Sec. IV, which have been done for isotropic perturbations. The effect of the lack of radial symmetry remains to be explored. Lastly, it is possible that the interaction between the graphene layer and the substrate is not uniform, due to the presence of charges and other defects within the substrate. The modeling of this kind of potential goes beyond the scope of this paper.

ACKNOWLEDGMENTS

S.V.K. thanks Alex Kitt for fruitful conversations and William Cullen for relevant suggestions. A.H.C.N. acknowledges DOE Grant No. DE-FG02-08ER46512 and ONR Grant No. MURI N00014-09-1-1063. F.G. acknowledges financial support from MICINN (Spain), Grants No. FIS2008-00124 and CONSOLIDER CSD2007-00010.

APPENDIX A: FULL SOLUTION FOR A GAUSSIAN BUMP: FLEXURAL MODES

In the main text, we analyzed the stability of a membrane on top of a Gaussian bump, which is pinned at the very top of the bump and reattaches to the substrate at a radius L. This was an assumption based on energetic arguments. The most general solution can have the membrane conforming to the substrate from the top up to a finite depinning radius R, and then reattaching at a radius L. In this case, the general solution Eq. (20) is valid for $R < r < L$, and all the coefficients H_i, $i = 0, \ldots, 3$, can be finite. These can be found by imposing the continuity of the solution and its first derivative both at R and L. Defining

$$\mathcal{H} = \frac{G_s e^{-\frac{L^2+R^2}{2\sigma^2}}}{\sigma^2[(L^2-R^2)^2 - 4L^2R^2(\log L - \log R)^2]},$$

we have

$$\begin{aligned}
H_0 &= \mathcal{H}\big[(L^2-R^2)(e^{\frac{L^2}{2\sigma^2}}L^2 - e^{\frac{R^2}{2\sigma^2}}R^2)\sigma^2 - 2e^{\frac{L^2}{2\sigma^2}}L^2R^2(R^2+2\sigma^2)\log L^2\big] \\
&\quad + \mathcal{H}L^2R^2\log R\big[2e^{\frac{R^2}{2\sigma^2}}\sigma^2 + e^{\frac{L^2}{2\sigma^2}}(L^2-R^2-2\sigma^2) - 2e^{\frac{R^2}{2\sigma^2}}L^2R^2(L^2+2\sigma^2)\log R\big] \\
&\quad + \mathcal{H}L^2R^2\log L\big[2e^{\frac{L^2}{2\sigma^2}}\sigma^2 + e^{\frac{R^2}{2\sigma^2}}(-L^2+R^2-2\sigma^2) + 2(e^{\frac{R^2}{2\sigma^2}}(L^2+2\sigma^2) + e^{\frac{L^2}{2\sigma^2}}(R^2+2\sigma^2))\log R\big], \\
H_1 &= -\mathcal{H}L^2R^2\big[(e^{\frac{L^2}{2\sigma^2}} - e^{\frac{R^2}{2\sigma^2}})(L^2-R^2) + (2e^{\frac{R^2}{2\sigma^2}}(L^2+2\sigma^2) - 2e^{\frac{L^2}{2\sigma^2}}(R^2+2\sigma^2))\log L\big] \\
&\quad + 2\mathcal{H}L^2R^2\big[e^{\frac{R^2}{2\sigma^2}}(L^2+2\sigma^2) - e^{\frac{L^2}{2\sigma^2}}(R^2+2\sigma^2)\big]\log R, \\
H_2 &= -2\mathcal{H}\big[(e^{\frac{L^2}{2\sigma^2}} - e^{\frac{R^2}{2\sigma^2}})(L^2-R^2)\sigma^2 - 2e^{\frac{L^2}{2\sigma^2}}L^2R^2\log L^2\big] - 2\mathcal{H}R^2\log R\big[2e^{\frac{R^2}{2\sigma^2}}\sigma^2 + e^{\frac{L^2}{2\sigma^2}}(L^2-R^2-2\sigma^2) - 2e^{\frac{R^2}{2\sigma^2}}L^2\log R\big] \\
&\quad - 2\mathcal{H}L^2\log L\big[2e^{\frac{L^2}{2\sigma^2}}\sigma^2 + e^{\frac{R^2}{2\sigma^2}}(-L^2+R^2-2\sigma^2) + 2(e^{\frac{L^2}{2\sigma^2}} + e^{\frac{R^2}{2\sigma^2}})R^2\log R\big], \\
H_3 &= -\mathcal{H}(L^2-R^2)\big[e^{\frac{R^2}{2\sigma^2}}(L^2+2\sigma^2) - e^{\frac{L^2}{2\sigma^2}}(R^2+2\sigma^2)\big] - 2\mathcal{H}L^2R^2\big[(e^{\frac{L^2}{2\sigma^2}} - e^{\frac{R^2}{2\sigma^2}})\log L - (e^{\frac{L^2}{2\sigma^2}} - e^{\frac{R^2}{2\sigma^2}})\log R\big].
\end{aligned} \tag{A1}$$

The total bending energy can be calculated as in the main text, taking into account that we now have three different regions of integration. The result, measured from the totally pinned configuration, is given by

$$\begin{aligned}
E_\kappa &= \kappa\pi\mathcal{H}\frac{(L^2-R^2)}{2\sigma^2}\big[-16e^{\frac{L^2+R^2}{2\sigma^2}}[L^2R^2 + (L^2+R^2)\sigma^2 + 2\sigma^4]\big] \\
&\quad + \kappa\pi\mathcal{H}\frac{(L^2-R^2)}{2\sigma^4}e^{\frac{R^2}{\sigma^2}}[L^6 - 2\sigma^4(R^2-8\sigma^2) - L^4(R^2-6S^2) + 2L^2\sigma^2(R^2+9S^2)] \\
&\quad + \kappa\pi\mathcal{H}\frac{(L^2-R^2)}{2\sigma^4}e^{\frac{L^2}{\sigma^2}}[R^6 + 2\sigma^2(3R^4+9R^2\sigma^2+8\sigma^4) - L^2(R^4-2R^2\sigma^2+2\sigma^4)] \\
&\quad + 8\kappa\pi\mathcal{H}\frac{L^2R^2(\log L - \log R)}{\sigma^2}e^{\frac{L^2+R^2}{2\sigma^2}}(L^2+R^2+4\sigma^2) \\
&\quad - 2\kappa\pi\mathcal{H}\frac{L^2R^2(\log L - \log R)}{\sigma^4}e^{\frac{R^2}{\sigma^2}}[4\sigma^2(L^2+2\sigma^2) + (L^4+2L^2\sigma^2+2\sigma^4)(\log L - \log R)]
\end{aligned}$$

$$+ 2\kappa\pi\mathcal{H}\frac{L^2R^2(\log L - \log R)}{\sigma^4}e^{\frac{L^2}{\sigma^2}}[-4\sigma^2(R^2+2\sigma^2) + (R^4+2R^2\sigma^2+2\sigma^4)(\log L - \log R)]. \tag{A2}$$

This bending energy together with the contact energy cost gives the plot shown in Fig. 10.

APPENDIX B: SOLUTION FOR A GAUSSIAN DEPRESSION AND BUMP: IN-PLANE MODES

A. Gaussian depression

We will call $u_r^<$ and $u_r^>$ the solutions of (38) for $0 \leqslant r \leqslant R$ and $r > R$, respectively. For $0 \leqslant r \leqslant R$, (37) is homogeneous and has a general solution of the kind

$$\frac{A_0}{r} + A_1 r.$$

The constant $A_0 \equiv 0$ for the solution to be regular at the origin, and A_1 is determined by the boundary conditions.

For $r > R$, the homogeneous solution is given by

$$\frac{C_0}{r} + C_1 r,$$

but in this case we get $C_1 \equiv 0$ by imposing that the displacements are 0 at infinity. C_0 is determined by boundary conditions. To obtain the general solution of (38) for $r > R$, we have to add a particular solution. This can be obtained by the ansatz solution:

$$u_r = \sum_m a_m r^m e^{-\frac{r^2}{\sigma^2}}. \tag{B1}$$

Substituting (B1) into the second line of (38) and using (39), we obtain

$$\sum_m a_m\left[\frac{4}{\sigma^4}r^{m+2} - \frac{4}{\sigma^2}(m+1)r^m + (m^2-1)r^{m-2}\right] = \frac{G_s^2}{\sigma^6}r^3 - \frac{G_s^2}{\sigma^4}\frac{(\lambda+3\mu)}{(\lambda+2\mu)}r. \tag{B2}$$

From here we see that there is a possible solution with $m = \pm 1$. By substituting in (B2), we obtain

$$a_1 = \frac{G_s^2}{4\sigma^2}, \qquad a_{-1} = \frac{G_s^2}{4}\frac{(\lambda+\mu)}{(\lambda+2\mu)}. \tag{B3}$$

The coefficients A_1 and C_0 are determined by imposing the continuity of the solution $u_r^>(R) = u_r^<(R)$ and of the in-plane stresses at R:

$$\sigma_{rr} = \lambda\left[\partial_r u_r + \frac{u_r}{r} + \frac{1}{2}(\partial_r h)^2\right] + 2\mu\left[\partial_r u_r + \frac{1}{2}(\partial_r h)^2\right], \tag{B4}$$

and hence the full solution is given by (40) in the main text.

B. Gaussian bump

As discussed in the main text, for a bump we approximate the membrane's profile in the detached region by the general solution given in the BD regime Eq. (20):

$$h(r) = G_s + \frac{H_2}{2}r^2 + H_3 r^2 \log r, \tag{B5}$$

where we have set $H_0 = G_s$ and $H_1 = 0$ as explained in Sec. III C. If we denote the reattachment radius as L, then the in-plane radial displacement u_r is given by

$$-(\lambda+2\mu)\left(\partial_r^2 u_r + \frac{\partial_r u_r}{r} - \frac{u_r}{r^2}\right) = \begin{cases} (\lambda+2\mu)\partial_r h\left(\partial_r^2 h\right) + \frac{\mu}{r}(\partial_r h)^2, & 0 \leqslant r \leqslant L \\ (\lambda+2\mu)\partial_r s\left(\partial_r^2 s\right) + \frac{\mu}{r}(\partial_r s)^2, & r > L \end{cases} \tag{B6}$$

together with the appropriate boundary conditions. The solutions for $0 \leqslant r \leqslant L$ and $r > L$ are given, respectively, by

$$\begin{aligned} u_r^<(r) &= C_1 r - \frac{r^3\left[-2H_1H_2(\lambda+\mu) + 2H_1^2(\lambda+3\mu) + H_2^2(\lambda+\mu)\right]}{16(\lambda+2\mu)} \\ &\quad + \frac{r^3 H_2 \log(r)\{H_2(\lambda+\mu) - 2[H_1 + H_2\log(r)](\lambda+3\mu)\}}{4(\lambda+2\mu)}, \\ u_r^>(r) &= \frac{C_0}{r} + \frac{G_s^2 e^{-\frac{r^2}{\sigma^2}}}{4(\lambda+2\mu)r}\left[(\lambda+\mu) + (\lambda+2\mu)\frac{r^2}{\sigma^2}\right]. \end{aligned} \tag{B7}$$

The parameters H_1, H_2, C_0, and C_1 are fixed by the boundary conditions, the continuity of the solution Eq. (B7) and its first derivative at $r = L$, and the continuity of the in-plane stress Eq. (B4), plus the continuity of the flexural field $h(L) = s(L)$. Imposing these result in two possible sets of solutions gives

$$
\begin{aligned}
C_0 &= -\frac{G_s^2 e^{-\frac{L^2}{\sigma^2}}(\lambda+\mu)\left(L^4+4L^2\sigma^2+8\sigma^4-8e^{\frac{L^2}{2\sigma^2}}\sigma^4+4e^{\frac{L^2}{\sigma^2}}\sigma^4\right)}{16(\lambda+2\mu)\sigma^4},\\
C_1 &= \frac{G_s^2 e^{-\frac{L^2}{\sigma^2}}\mu\left(L^4+5L^2\sigma^2-4e^{\frac{L^2}{2\sigma^2}}L^2\sigma^2+8\sigma^4-16e^{\frac{L^2}{2\sigma^2}}\sigma^4+8e^{\frac{L^2}{\sigma^2}}\sigma^4\right)}{4L^2(\lambda+2\mu)\sigma^4},\\
H_1 &= \frac{2G_s e^{-\frac{L^2}{2\sigma^2}}\left(-\sigma^2+e^{\frac{L^2}{2\sigma^2}}\sigma^2-L^2\log(L)-2\sigma^2\log(L)+2e^{\frac{L^2}{2\sigma^2}}\sigma^2\log(L)\right)}{L^2\sigma^2},\\
H_2 &= \frac{G_s e^{-\frac{L^2}{2\sigma^2}}\left(-L^2-2\sigma^2+2e^{\frac{L^2}{2\sigma^2}}\sigma^2\right)}{L^2\sigma^2},
\end{aligned}
\tag{B8}
$$

$$
\begin{aligned}
C_0 &= -\frac{G_s^2 e^{-\frac{L^2}{\sigma^2}}(\lambda+\mu)\left(L^4+4L^2\sigma^2+8\sigma^4-8e^{\frac{L^2}{2\sigma^2}}\sigma^4+4e^{\frac{L^2}{\sigma^2}}\sigma^4\right)}{16(\lambda+2\mu)\sigma^4},\\
C_1 &= \frac{G_s^2 e^{-\frac{L^2}{\sigma^2}}\mu\left(L^4-3L^2\sigma^2+4e^{\frac{L^2}{2\sigma^2}}L^2\sigma^2+8\sigma^4-16e^{\frac{L^2}{2\sigma^2}}\sigma^4+8e^{\frac{L^2}{\sigma^2}}\sigma^4\right)}{4L^2(\lambda+2\mu)\sigma^4},\\
H_1 &= \frac{2G_s e^{-\frac{L^2}{2\sigma^2}}\left(-\sigma^2+e^{\frac{L^2}{2\sigma^2}}\sigma^2+L^2\log(L)-2\sigma^2\log(L)+2e^{\frac{L^2}{2\sigma^2}}\sigma^2\log(L)\right)}{L^2\sigma^2},\\
H_2 &= \frac{G_s e^{-\frac{L^2}{2\sigma^2}}\left(L^2-2\sigma^2+2e^{\frac{L^2}{2\sigma^2}}\sigma^2\right)}{L^2\sigma^2}.
\end{aligned}
\tag{B9}
$$

The total energy can be calculated from the general expression Eq. (37) by use of Eq. (B7) and Eq. (B8) and Eq. (B9), resulting in the two energy profiles plotted in Fig. 15.

*Present address: Dahlem Center for Complex Quantum Systems, Freie Universitaet Arnimallee 14, 14195 Berlin, Germany.

[1] D. Nelson, S. Weinberg, and T. Piran, *Statistical Mechanics of Membranes and Surfaces*, 2nd ed. (World Scientific, Singapore, 2004), and references therein.

[2] K. S. Novoselov, A. K. Geim, S. V. Morozov, D. Jiang, Y. Zhang, S. V. Dubonos, I. V. Gregorieva, and A. A. Firsov, Science **306**, 666 (2004).

[3] K. S. Novoselov, A. K. Geim, S. V. Morozov, D. Jiang, M. I. Katsnelson, I. V. Grigorieva, S. V. Dubonos, and A. A. Firsov, Nature (London) **438**, 197 (2005).

[4] Y. Zhang, Y.-W. Tan, H. L. Stormer, and P. Kim, Nature (London) **438**, 201 (2005).

[5] K. Geim and K. S. Novoselov, Nat. Mater. **6**, 183 (2007), and references therein.

[6] S. V. Morozov, K. S. Novoselov, M. I. Katsnelson, F. Schedin, L. A. Ponomarenko, D. Jiang, and A. K. Geim, Phys. Rev. Lett. **97**, 016801 (2006).

[7] S. V. Morozov, K. S. Novoselov, M. I. Katsnelson, F. Schedin, D. C. Elias, J. A. Jaszczak, and A. K. Geim, Phys. Rev. Lett. **100**, 016602 (2008).

[8] J.-H. Chen, C. Jang, S. Xiao, M. Ishigami, and M. S. Fuhrer, Nat. Nanotech. **3**, 206 (2008).

[9] J. C. Meyer, A. K. Geim, M. I. Katsnelson, K. S. Novoselov, T. J. Booth, and S. Roth, Nature (London) **446**, 60 (2007).

[10] A. H. Castro Neto, F. Guinea, N. M. R. Peres, K. S. Novoselov, and A. K. Geim, Rev. Mod. Phys. **81**, 109 (2009), and references therein.

[11] M. Ishigami, J. H. Chen, W. G. Cullen, M. S. Fuhrer, and E. D. Williams, Nano Lett. **7**, 1643 (2007).

[12] E. Stolyarova, K. T. Rim, S. Ryu, J. Maultzsch, P. Kim, L. E. Brus, T. F. Heinz, M. S. Hybertsen, and G. W. Flynn, Proc. Natl. Acad. Sci. (USA) **104**, 9209 (2007).

[13] V. Geringer, M. Liebmann, T. Echtermeyer, S. Runte, M. Schmidt, R. Rückamp, M. C. Lemme, and M. Morgenstern, Phys. Rev. Lett. **102**, 076102 (2009).

[14] S. Scharfenberg, D. Z. Rocklin, C. Chialvo, R. L. Weaver, P. M. Goldbart, and N. Mason, e-print arXiv:1006.3037.

[15] P. M. Chaikin and T. C. Lubensky, *Principles of Condensed Matter Physics* (Cambridge University Press, Cambridge, 2000), and references therein.

[16] P. S. Swain and D. Andelman, Langmuir **15**, 8902 (1999).

[17] J. Sabio, C. Seoánez, S. Fratini, F. Guinea, A. H. Castro Neto, and F. Sols, Phys. Rev. B **77**, 195409 (2008).

[18] A. Fasolino, J. H. Los, and M. Katsnelson, Nat. Mater. **6**, 858 (2007).

[19] K. V. Zakharchenko, M. I. Katsnelson, and A. Fasolino, Phys. Rev. Lett. **102**, 046808 (2009).

[20] D. R. Nelson and L. Peliti, J. Phys. C **48**, 1085 (1987).

[21] J. Atalaya, A. Isacsson, and J. M. Kinaret, Nano Lett. **8**, 4196 (2008).

[22] J. H. Los, M. I. Katsnelson, O. V. Yazyev, K. V. Zakharchenko, and A. Fasolino, Phys. Rev. B **80**, 121405 (2009).

[23] L. D. Landau and E. M. Lifshitz, *Theory of Elasticity*, Vol. 7, 3rd ed. (Butterworth-Heinemann, Oxford, 1986).

[24]S. P. Timoshenko and S. Woinowsky-Kreiger, *Theory of Plates and Shells* (McGraw-Hill, Singapore, 1987).
[25]E. Prada, P. San-José, G. León, M. M. Fogler, and F. Guinea, Phys. Rev. B **81**, 161402 (2010).
[26]E. H. Hwang, S. Adam, and S. Das Sarma, Phys. Rev. Lett. **98**, 186806 (2007).
[27]K. Bolotin, K. Sikes, Z. Jiang, M. Klima, G. Fudenberg, J. Hone, P. Kim, and H. Stormer, Solid State Commun. **146**, 351 (2008).
[28]E. V. Castro, H. Ochoa, M. I. Katsnelson, R. V. Gorbachev, D. C. Elias, K. S. Novoselov, A. K. Geim, and F. Guinea, e-print arXiv:1008.2522.
[29]E. Mariani and F. von Oppen, e-print arXiv:1008.1631.
[30]E. Stolyarova *et al.*, Nano Lett. **9**, 332 (2009).
[31]N. Levy, S. Burke, K. L. Meaker, M. Panlasigui, A. Zettl, F. Guinea, A. H. C. Neto, and M. F. Crommie, Science **329**, 544 (2010).
[32]K. S. Novoselov (private communication).
[33]N. Agraït (private communication).
[34]O. Pierre-Louis, Phys. Rev. E **78**, 021603 (2008).
[35]T. Li and Z. Zhang, Nanoscale Res. Lett. **5**, 169 (2010).
[36]T. Li and Z. Zhang, J. Phys. D **43**, 075303 (2010).
[37]P. S. Swain and D. Andelman, Phys. Rev. E **63**, 051911 (2001).
[38]T. Auth, S. A. Safran, and N. S. Gov, Phys. Rev. E **76**, 051910 (2007).